Am J Physiol Cell Physiol 306: C441–C449, 2014.
First published October 23, 2013; doi:10.1152/ajpcell.00236.2013.

Rab11a-positive compartments in proximal tubule cells sort fluid-phase and membrane cargo

Polly E. Mattila,[1]* Venkatesan Raghavan,[1]* Youssef Rbaibi,[1]* Catherine J. Baty,[2] and Ora A. Weisz[1,2]

[1]*Renal-Electrolyte Division, Department of Medicine, University of Pittsburgh, Pittsburgh, Pennsylvania; and* [2]*Department of Cell Biology, University of Pittsburgh, Pittsburgh, Pennsylvania*

Submitted 6 August 2013; accepted in final form 21 October 2013

Mattila PE, Raghavan V, Rbaibi Y, Baty CJ, Weisz OA. Rab11a-positive compartments in proximal tubule cells sort fluid-phase and membrane cargo. *Am J Physiol Cell Physiol* 306: C441–C449, 2014. First published October 23, 2013; doi:10.1152/ajpcell.00236.2013.—The proximal tubule (PT) reabsorbs the majority of sodium, bicarbonate, and chloride ions, phosphate, glucose, water, and plasma proteins from the glomerular filtrate. Despite the critical importance of endocytosis for PT cell (PTC) function, the organization of the endocytic pathway in these cells remains poorly understood. We have used immunofluorescence and live-cell imaging to dissect the itinerary of apically internalized fluid and membrane cargo in polarized primary cultures of PTCs isolated from mouse kidney cortex. Cells from the S1 segment could be distinguished from those from more distal PT segments by their robust uptake of albumin and comparatively low expression of γ-glutamyltranspeptidase. Rab11a in these cells is localized to variously sized spherical compartments that resemble the apical vacuoles observed by electron microscopy analysis of PTCs in vivo. These Rab11a-positive structures are highly dynamic and receive membrane and fluid-phase cargo. In contrast, fluid-phase cargoes are largely excluded from Rab11a-positive compartments in immortalized kidney cell lines. The unusual morphology and sorting capacity of Rab11a compartments in primary PTCs may reflect a unique specialization of these cells to accommodate the functional demands of handling a high endocytic load.

proximal tubule; megalin; apical; endocytosis; Rab11; recycling endosome

THE KIDNEY IS THE PRINCIPAL organ involved in the regulation of acid-base balance, blood pressure, electrolyte balance, and blood plasma composition in higher mammals. The nephron is the fundamental functional unit of the kidney and is divided into five functional segments: glomerulus, proximal tubule (PT), loop of Henle, distal tubule, and collecting duct. The PT is responsible for reabsorption of ~70% of sodium, bicarbonate, and chloride ions, phosphate, glucose, and water from the glomerular filtrate (reviewed in Refs. 10 and 38). The PT is further divided into S1, S2, and S3 segments on the basis of physiological, ultrastructural, and functional differences (20). The S1 segment is characterized by high expression of megalin, whereas the PT marker γ-glutamyltranspeptidase (γ-GT) is expressed at highest concentration in S2 and S3 cells (5, 18, 27).

The lumen of the PT is lined by polarized epithelial cells that maintain a high capacity for apical endocytosis. A primary function of these cells is retrieval of serum components with a molecular weight below the glomerular filtration limit of ~60,000 that enter the lumen of the PT. Many of these proteins and small molecules are ligands for the apically expressed multiligand receptors megalin and cubilin (reviewed in Ref. 9). Failure to retrieve filtered proteins results in low-molecular-weight proteinuria, also known as tubular proteinuria. Defects in the expression or trafficking of megalin or cubilin result in tubular proteinuria, as observed in patients with Dent disease, Lowe syndrome, Imerslund-Gräsbeck syndrome, and Donnai-Barrow syndrome (reviewed in Ref. 28).

Although endocytosis is critical for normal PT function, little is known about the endocytic pathway in these cells. Much of our understanding of the apical endocytic pathway in these cells comes from electron microscopy studies examining the internalization pathway of fluid-phase and membrane tracers (3, 16, 17, 29, 30). These tracers are internalized into clathrin-coated vesicles that bud from the base of the brush border microvilli and are thought to fuse with a subapical network of tubules (30). Fast recycling to the apical surface may occur from these sites. These fluid-phase and membrane tracers have access to large apical compartments, termed apical vacuoles (AVs), within 1–15 min after internalization (16, 17, 30). Tubule-like structures that are believed to carry recycling proteins back to the apical surface can be observed emanating from these AVs (11, 16, 17). Nonrecycling proteins are thought to be transported to lysosomes for degradation and/or transcytosed to the basolateral membrane (14, 15). Although the endocytic structures accessed by markers have been described, the identity of these structures remains unknown. Notably, the organization of this pathway in PT cells (PTCs) differs considerably from that of the apical recycling pathway described in cells derived from different kidney segments (21, 40). Therefore, we sought to examine the itinerary of apically internalized albumin in a PTC model that retains essential features of this endocytic pathway.

We have developed a primary cell culture model of mouse PTCs to study the organization and molecular identity of compartments along the apical endocytic pathway. Cultured primary cells form a differentiated polarized monolayer that maintains characteristics of the PT segments from which they were derived. We have investigated the structure and distribution of known endocytic compartment markers in our primary culture system and determined the pathway for internalization and sorting of a fluid-phase marker and the megalin/cubilin ligand albumin. Our studies suggest that the Rab11a-positive compartments represent the AVs reported in ultrastructural studies of PTs and that these structures receive and sort fluid and membrane cargoes. The unique organization of the apical

* P. E. Mattila, V. Raghavan, and Y. Rbaibi contributed equally to this work.

Address for reprint requests and other correspondence: O. A. Weisz, Univ. of Pittsburgh School of Medicine, Renal-Electrolyte Division, 3550 Terrace St., Pittsburgh, PA 15261 (e-mail: weisz@pitt.edu).

endocytic pathway in PTCs likely reflects the specific functional demands of this kidney segment.[1]

MATERIALS AND METHODS

Reagents. Reagents for cell culture and analysis were obtained as follows: collagen I from EMD-Millipore (Billerica, MA), bovine collagen IV from Rockland Immunochemicals (Gilbertsville, PA), DMEM/Ham's F-12 medium (DMEM/F-12) and media additives (insulin, transferrin, selenium, and dexamethasone) from Sigma-Aldrich (St. Louis, MO), permeable supports (0.4-μm-pore Transwell inserts) from Corning (Corning, NY), collagenase type II from Worthington (Lakewood, NJ), paraformaldehyde from Electron Microscopy Sciences (Hatfield, PA), and trypsin (catalog no. 12563-029) from GIBCO Life Technologies (Carlsbad, CA).

Isolation, culture, and transfection of PTCs. The protocol for isolating PTCs from 6- to 8-wk-old male mice was adapted from a previously published method (33). Mice were euthanized in accordance with procedures approved by the University of Pittsburgh Institutional Animal Care and Use Committee, and the kidneys were removed and placed in ice-cold renal PTC (RPTC) buffer (in mM: 115 NaCl, 24 $NaHCO_3$, 5 KCl, 1.5 $CaCl_2$, 10 $MgSO_4$, 2 KH_2PO_4, 5 glucose, and 50 mannitol, pH 7.4). The kidney capsule was removed, the kidney was cut sagittally, and the medulla was removed. The cortex was minced under sterile conditions into 1-mm pieces and gently washed to remove debris, and collagenase type II and BSA were added to achieve a final concentration of 0.1% and 0.5%, respectively. The tissue was digested for 45 min at 37°C, and digestion was stopped by addition of ice-cold RPTC buffer with 5% BSA for 5 min on ice. The tissue was centrifuged for 30 s and resuspended in 20 ml of RPTC buffer. The suspension was sequentially passed through a series of stackable metal sieves with 180-, 90-, and 45-μm pores, respectively (Alfa Aesar USA standard sieve, Ward Hill, MA). The final isolate was collected, resuspended in DMEM/F-12 + L-glutamine-10% FBS, and plated on collagen I-coated plates or collagen IV-coated permeable supports. The medium was replaced with RPTC medium with 1% FBS (DMEM/F-12 supplemented with 5 μg/ml insulin, 0.02 μg/ml dexamethasone, 0.01 μg/ml selenium, 5 μg/ml transferrin, 2 mM L-glutamine, 10^{-9} M triiodothyronine, and 1% FBS) after 24 h, and the cells were used for experiments as described in the timeline in Fig. 1*A*. Cells were transfected as follows for live-cell-imaging experiments: plasmids encoding *S*-nitroso-*N*-acetyl-penicillamine (SNAP)-Rab11a (0.25–0.5 μg) and minimegalin-green fluorescent protein (GFP, 0.5 μg) were suspended in 63 μl of OptiMEM (GIBCO) and incubated at ambient temperature for 5 min. One microliter of Lipofectamine 2000 was resuspended in 63 μl of OptiMEM and incubated at ambient temperature for 5 min. Lipofectamine and DNA suspensions were mixed and incubated at ambient temperature for 20 min. RPTCs were trypsinized, and 2×10^5 cells were resuspended with transfection mix and plated onto collagen IV-coated dishes (MatTek, Ashland, MA). The medium was changed 6 h postplating to avoid lipid toxicity.

Indirect immunofluorescence. Anionic lysine-fixable rhodamine-dextran (10,000 mol wt) and Alexa Fluor 555- and Alexa Fluor 647-conjugated BSA were obtained from Life Technologies. Rhodamine-conjugated wheat germ agglutinin (WGA) was from Vector Laboratories (Burlingame, CA). Rabbit anti-γ-GT antibody (1:100 dilution) and rat anti-zonula occludens 1 (ZO)-1 monoclonal antibody were gifts from Dr. Rebecca Hughey and Dr. Gerard Apodaca, respectively. Polyclonal anti-early endosome antigen 1 (EEA1) antibody (1:250 dilution) was obtained from Thermo Fisher (Pittsburgh, PA), and monoclonal anti-E-cadherin antibody (1:200 dilution) from BD Transduction Laboratories (San Jose, CA). Cells plated on permeable supports were transfected on *day 4* and fixed on *day 7* in 4% paraformaldehyde-100 mM sodium cacodylate, pH 7.4. Filters were incubated in 0.1% Triton X-100 in 75 mM NH_4Cl_2-20 mM glycine-PBS for 10 min, washed, and blocked in 1% BSA-0.1% saponin for 1 h. Primary antibodies were added in 0.5% BSA-0.025% saponin in PBS for 1 h at ambient temperature, and filters were washed three times with 0.5% BSA-0.025% saponin in PBS. Secondary Alexa Fluor-conjugated antibodies (Invitrogen) were used at a dilution of 1:500 for 30 min, and TO-PRO-3 (1:1,000 dilution; Molecular Probes, Eugene, OR) was included where indicated. The filters were washed and then mounted onto glass slides with ProLong Gold (Life Technologies). Imaging was performed on a Leica SP5 confocal microscope (×100/1.5 numerical aperture objective) and processed using Adobe Photoshop CS4.

PCR detection of murine megalin mRNA. mRNA was extracted using the Ambion RNAqueous phenol-free total RNA isolation kit (Life Technologies). One microgram of RNA was used for synthesis of cDNA using Moloney's murine leukemia virus reverse transcriptase (Life Technologies) according to the manufacturer's recommendations. PCR was performed in 50-μl reactions using the Bio-Rad iCycler and Phusion High-Fidelity PCR system (New England Biolabs, Ipswich, MA). Primer sets against megalin were designed using PrimerQuest on the Integrated DNA Technologies website: 5′-CTA-ACCAAGGCAGGACGTTTC-3′ (forward) and 5′-TCCACCGTG-GACACAAGTAAA-3′ (reverse) for megalin and 5′-ACCTTCA-ACTCCATCATGAAG-3′ (forward) and 5′-CTGCTGGAAGGTG-GACAG-3′ (reverse) for actin. Denaturing temperature was 95°C, annealing temperature was 54.5°C, and extension temperature was 72°C for 25 amplification cycles.

Transmission electron microscopy. Cells grown on collagen IV-coated permeable supports were fixed in 2.5% glutaraldehyde for 1 h, washed with PBS, postfixed for 1 h in 1% OsO_4 with 1% potassium ferricyanide, and washed with PBS. After dehydration in a graded series of 30–100% alcohol, the filters were infiltrated with pure EPON three times for 1 h each and then cut and embedded in pure EPON. After 24 h at 37°C, samples were polymerized at 60°C for 48 h. Samples were sectioned, mounted on grids, stained with 2% uranyl acetate and then lead citrate, and examined using a transmission electron microscope (JEM-1011, JEOL).

Live-cell imaging of PTCs. Isolated PTCs grown on collagen I-coated dishes were transfected with the indicated combination of plasmids [mCherry-Rab11a, SNAP-tagged Rab11a, and GFP-tagged minimegalin (12, 24)] and plated on collagen I-coated dishes (MatTek). At 3 days posttransfection, PTCs were incubated as indicated with SNAP-Cell TMR-Star or SNAP-Cell 505 (New England Biolabs; 3 μM final concentration) for 30 min at 37°C to label Rab11a-SNAP. Cells were then incubated with serum-free RPTC buffer containing rhodamine-dextran (1 mg/ml) and/or Alexa Fluor 647-albumin at 37°C, and live-cell time-lapse microscopy was performed. Live-cell imaging to visualize SNAP-tagged Rab11a dynamics in RPTCs was performed using the Andor revolution XD platform. A live-cell chamber compatible with the inverted spinning-disk microscope was used to maintain a temperature of 37°C and P_{CO_2} of 5%. Images were captured using a 12-bit electron-multiplying charge-coupled device iXON camera controlled by the Andor iQ interface. Images were continuously acquired over a 10-min period. Live-cell imaging to visualize cargo sorting from the Rab11a-positive compartments was performed using the Leica TCS SP5 platform. A live-cell chamber compatible with the inverted laser-scanning microscope was used to maintain a temperature of 37°C. Images were captured using a 16-bit dynamic hybrid detector in 5-s intervals over 5 min. Images were exported in a 16-bit TIFF format for qualitative analyses. Time-lapse images were reconstructed using Imaris (Bitplane), and a 3×3 median filter was applied to the images. Fission and fusion events were recorded as audio-video interleave. Signal overlap of dextran, albumin, and megalin with the Rab11a-positive compartments was computed using MetaMorph (Molecular Devices, Sunnyvale, CA). Integrated morphometry analysis was used to construct a mask based

[1] This article is the topic of an Editorial Focus by Curtis T. Okamoto (29a).

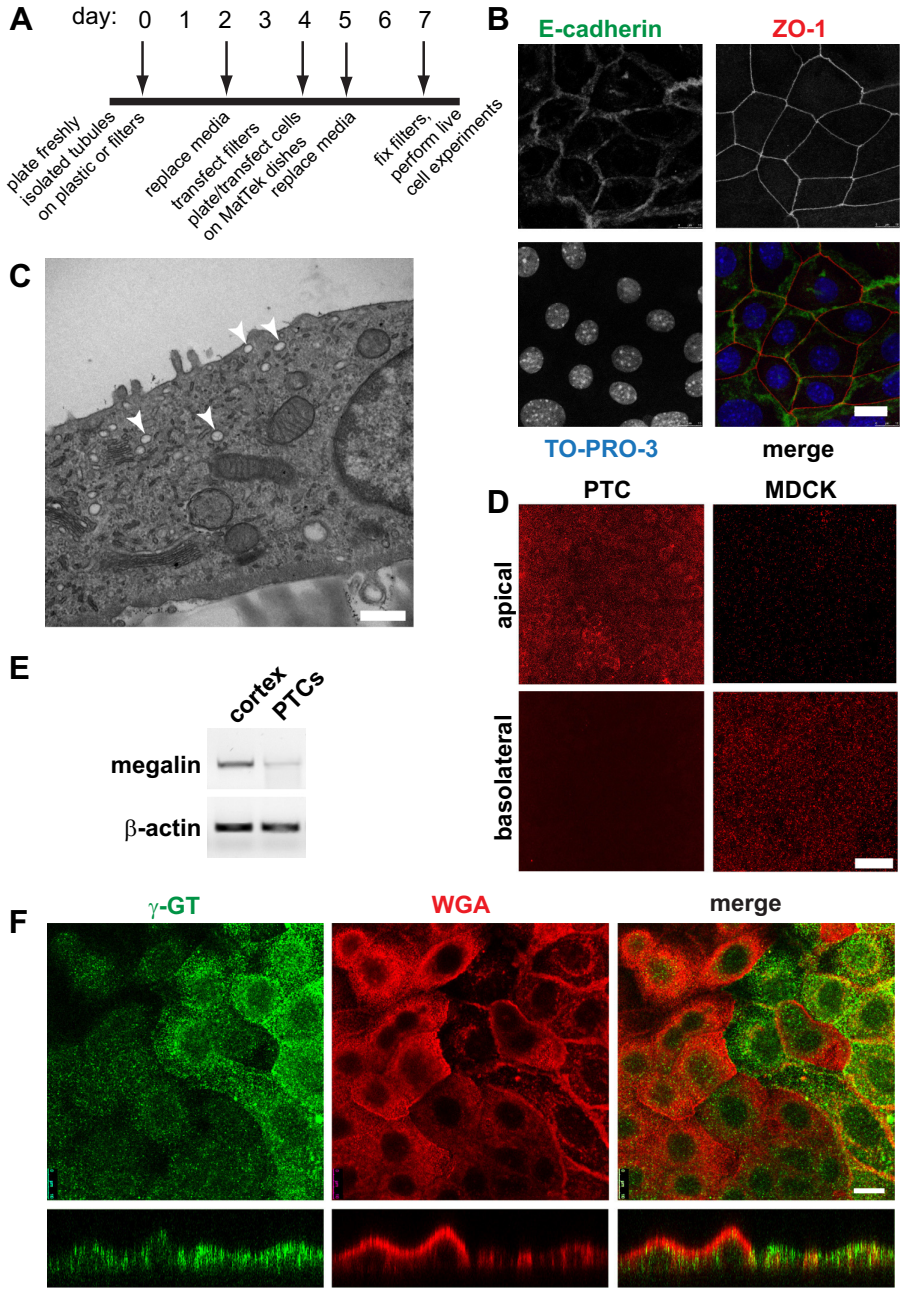

Fig. 1. Characterization of primary proximal tubule cell (PTC) cultures. *A*: timeline of cell-plating schedule after isolation of PTCs from mouse kidney cortex. *B*: PTCs grown on permeable supports were fixed and processed for indirect immunofluorescence to detect the lateral adherens junction marker E-cadherin (green), the tight junction marker zonula occludens 1 (ZO-1; red), and nuclei using TO-PRO-3 (blue). Scale bar, 10 μm. *C*: PTCs grown on permeable supports were processed for transmission electron microscopy. Arrowheads denote subapical structures that may correspond to apical vacuoles observed in vivo. Scale bar, 500 nm. *D*: filter-grown PTCs or Madin-Darby canine kidney (MDCK) cells were incubated with apically or basolaterally added rhodamine-dextran (1 mg/ml) for 20 min and processed for immunofluorescence. PTCs internalized dextran primarily from the apical surface, whereas the opposite was observed for MDCK cells. Scale bar, 15 μm. *E*: RT-PCR was performed to detect megalin expression from reverse-transcribed mRNA isolated from mouse cortex or from PTCs after 7 days in culture. β-Actin is included as a loading control. *F*: filter-grown PTCs were incubated with rhodamine-conjugated wheat germ agglutinin (WGA) for 30 min (red), fixed, and then processed to detect γ-glutamyltranspeptidase (γ-GT; green). Cells were analyzed by confocal microscopy, and individual optical sections and *xz* reconstructions are shown. Note that cells expressing higher levels of γ-GT bind to and internalize less WGA and are markedly flatter in cross section. Scale bar, 10 μm.

on area thresholding. The integrated density overlap of megalin and albumin over the Rab11a-positive compartments was computed using the colocalization package.

RESULTS

Primary cultures of mouse PT are polarized and express PT markers. To generate primary PTC cultures, renal tubules isolated from mouse kidney cortex were plated on collagen I-coated plastic or directly onto collagen IV-coated permeable supports. A timeline of the isolation and plating schedule is shown in Fig. 1*A*. Cells plated on plastic migrated from these tubules over several days and formed proliferating islands of cells that eventually coalesced to form a confluent monolayer. Similarly, tubules plated directly onto collagen IV-coated permeable supports formed confluent monolayers within several days, as assessed using 4′,6-diamidino-2-phenylindole staining (not shown). Cells in these monolayers were polarized as assessed by indirect immunofluorescence to visualize the tight junction marker ZO-1 (Fig. 1*B*). Moreover, the adherens junction marker E-cadherin localized exclusively to the lateral domains of these cells (Fig. 1*B*).

PTCs in vivo are characterized by the presence of highly regular and tall apical microvilli, as well as numerous AVs that receive internalized fluid and membrane markers (3, 30). To test whether these structures are retained in our primary cultures, freshly isolated PTCs cultured on permeable supports for 7 days were fixed and processed for transmission electron microscopy (see MATERIALS AND METHODS). In contrast to PTCs in vivo, our cultured cells were fairly flat and had only a few scattered microvilli (Fig. 1*C*). Tight junctions were readily

detected between adjacent cells, as predicted by our ZO-1 staining in Fig. 1*C* (not shown). This morphology is similar to that reported in numerous other studies of primary cultures isolated using similar approaches (2, 19, 33). Notably, however, we did observe large vacuolar structures near the apical surface of many cells (arrowheads in Fig. 1*C*). We speculate that these structures may represent the AVs described in vivo from which internalized apical cargo is recycled (3, 16, 17, 29, 30).

A unique characteristic of PTCs is high capacity for apical endocytosis. To test this, we added the fluid-phase marker rhodamine-dextran to the apical or basolateral chamber of filter-grown PTCs and compared the extent of uptake after 20 min. As shown in Fig. 1*D*, rhodamine-dextran was internalized to a much greater extent from the apical than basolateral surface in PTCs (Fig. 1*D*). In contrast, this marker was endocytosed primarily from the basolateral surface of Madin-Darby canine kidney (MDCK) cells, consistent with prior observations that basolateral internalization of membrane and fluid is more robust than apical endocytosis in these cells (4, 31).

We next examined the expression of PT-specific markers in our primary cell cultures. PCR amplification of reverse-transcribed mRNA confirmed that primary cultures continued to express the PT marker megalin, albeit at lower levels than in freshly isolated kidney cortex (Fig. 1*E*). Indirect immunofluorescence using antibodies directed against γ-GT revealed strong staining in a subset of cells, consistent with the presence of cells derived from S2 and S3 segments of the PT (Fig. 1*F*). Interestingly, when cells were incubated at 37°C with rhodamine-WGA prior to fixation and staining with anti-γ-GT antibody, we observed considerably more robust surface binding and internalization of WGA in the population of cells expressing low levels of γ-GT (Fig. 1*F*). As revealed by *xz* reconstructions of confocal stacks, the population of cells binding to WGA was typically taller than the fraction expressing higher levels of γ-GT. These studies also confirmed γ-GT staining primarily at the apical surface of PTCs, consistent with its known distribution in vivo.

A subset of PT-derived cells internalize apical albumin with high efficiency. The presence of at least two distinct populations of cells distinguished by γ-GT expression and WGA binding/uptake suggests that our cell culture model contains cells derived from all segments of the PT (S1, S2, and S3). PTCs in the S1 segment preferentially express megalin and cubilin, which function to reabsorb proteins and small molecules from the glomerular filtrate via receptor-mediated endocytosis (27). We therefore tested whether endocytosis of the megalin/cubilin ligand albumin is preferentially enriched in primary cells expressing lower levels of γ-GT. Control experiments confirmed that, similar to rhodamine-dextran (Fig. 1*D*), albumin was internalized almost exclusively from the apical surface of PTCs (not shown). Filter-grown cells were incubated for 30 min at 37°C with apically added 40 μg/ml Alexa Fluor 647-labeled albumin [well below the reported K_d of 1.25 mg/ml in human PT HK-2 cells (15)] and then washed, fixed, and stained with anti-γ-GT antibody. In Fig. 2, internalized albumin was observed in a subpopulation of cells and in spherical structures of varying sizes. Notably, the cells that most robustly internalized albumin uniformly had lower levels of γ-GT expression. Together, these data are consistent with the conclusion that the cells that efficiently internalize albumin are derived from the S1 segment, while the higher-γ-GT-expressing cells more closely resemble those of the S2 and S3 segments.

Characterization of endocytic compartments in albumin-internalizing PTCs. In the "classical" model of the endocytic pathway, dissociation of internalized ligands from their membrane receptors is promoted by the acidic pH of early endosomes (39). Subsequently, membrane receptors are segregated from these fluid-phase ligands by sequestration into membrane-rich/volume-poor tubules that emanate from early endosomes (13). These tubules can fuse directly with the cell surface (known as "fast recycling") or coalesce to form recycling endosomes. The continual depletion of membrane proteins from early endosomes generates spherical remnants enriched in fluid-phase cargo that gradually mature into late endosomes, which ultimately deliver their content to lysosomes.

Although PTCs in vivo are highly endocytically active, little is known about the identity of apical endocytic pathway compartments in cells derived from this renal segment. To investigate the organization of endocytic components in the PT, we examined the distribution of known markers of endocytic organelles (endogenously expressed or transiently transfected) in our culture model (Fig. 3). To focus selectively on the subpopulation of cells that express high levels of megalin/cubilin, we incubated filters with apically added Alexa Fluor 555-albumin (40 μg/ml) for 30 min prior to fixation and subsequent processing. Cells were imaged by confocal microscopy, and a single optical section for each marker is shown. To more easily visualize total cellular albumin uptake, we show maximal projections of the albumin fields.

To label early endosomes, we stained cells with antibodies against EEA1 (Fig. 3*A*) or expressed the early endosome marker GFP-Rab5 (Fig. 3*B*) in our cultures. Both of these markers localized to numerous small punctate structures, con-

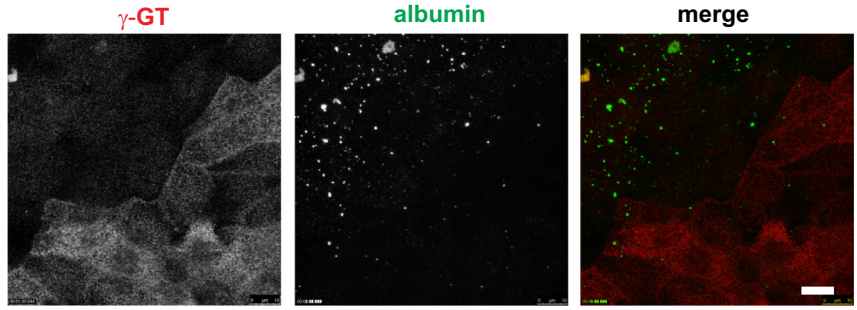

Fig. 2. A subset of PT-derived cells internalize apical albumin with high efficiency. Filter-grown PTCs were incubated with 40 μg/ml Alexa Fluor 647-albumin (pseudocolored green) added apically for 30 min, fixed, and then processed to detect γ-GT (red). An individual optical section for γ-GT, a maximum projection of albumin distribution, and merged images are shown. Note that cells with robust albumin internalization express comparatively low levels of γ-GT. Scale bar, 10 μm.

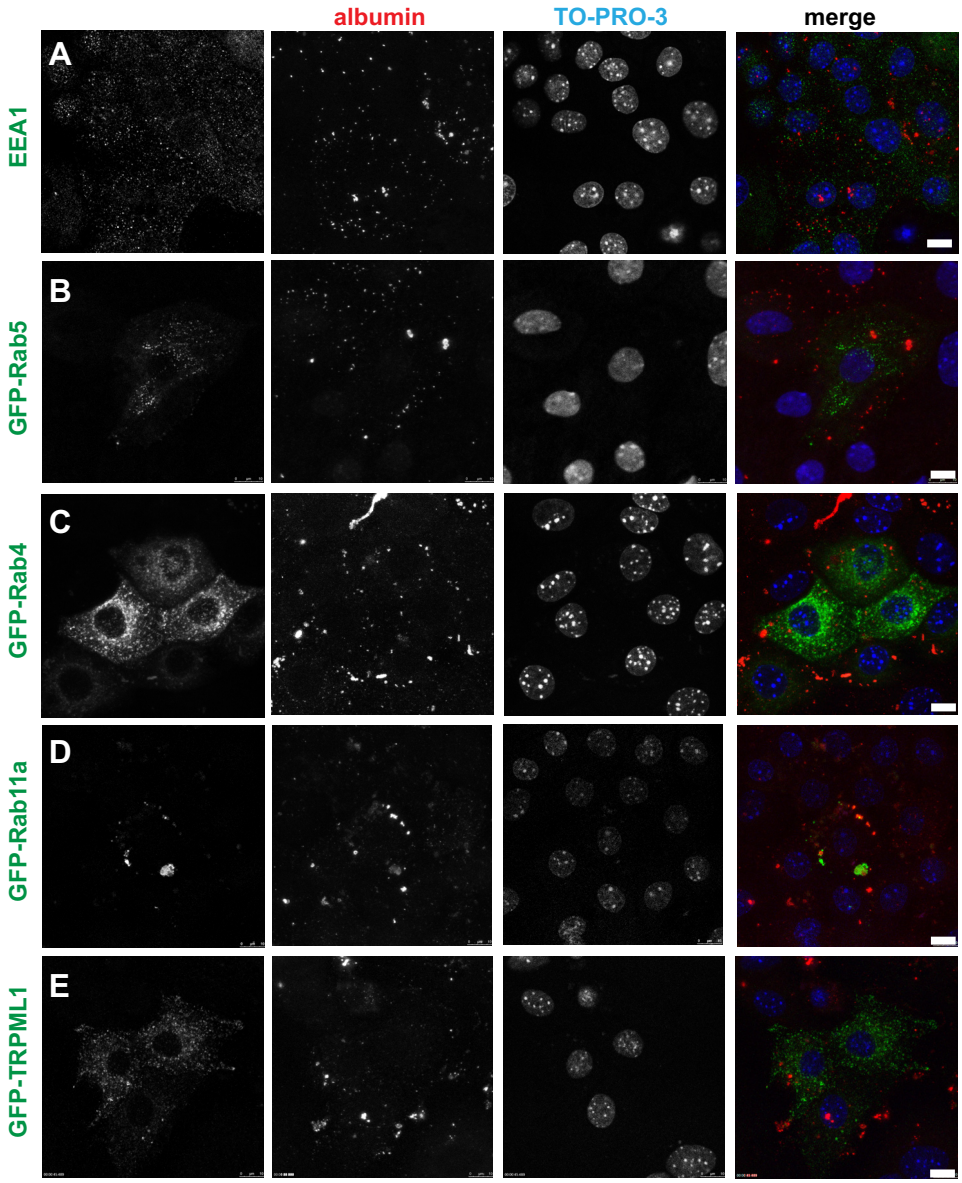

Fig. 3. Endocytic marker distribution in PTCs. Filter-grown PTCs [transfected with the indicated green fluorescent protein (GFP)-tagged markers where indicated] were incubated with 40 μg/ml Alexa Fluor 555-albumin added apically for 30 min (red), fixed, and then processed for immunofluorescence. Maximal projections of albumin labeling are shown to highlight the endocytically active cells, along with a single optical slice showing distribution of endocytic/lysosomal markers and the nuclear stain TO-PRO-3. Scale bars, 10 μm. EEA1, early endosome antigen 1; TRPML1, transient receptor potential cation channel mucolipin subfamily, member 1.

sistent with the known morphology of early endosomes. Next, we examined the distribution of GFP-Rab4, a protein that mediates fast recycling from early endosomes (34). Similar to its localization in HeLa cells (25), GFP-Rab4 staining was concentrated in juxtanuclear compartments (Fig. 3*C*). By contrast, GFP-Rab11a was present on discrete spherical compartments with a broad range of sizes that were distributed randomly throughout the cytoplasm (Fig. 3*D*). These compartments are reminiscent of the AVs described in vivo and sometimes contained internalized albumin. Finally, using the marker GFP-transient receptor potential cation channel mucolipin subfamily, member 1, we identified late endosomes and lysosomes (26, 37) (Fig. 3*E*). Similar to its distribution in other cell types, this protein localized to small spherical structures distributed throughout the cytoplasm.

Highly dynamic Rab11a-positive structures in PTCs mediate cargo sorting. In the context of the traditional model for endocytosis described above, the presence of Rab11a on large spherical structures that resemble AVs and contain albumin was surprising. In MDCK cells, Rab11a localizes to a condensed network of subapical recycling endosomes (8). Moreover, internalized fluid-phase markers have been reported to be excluded from Rab11a-positive compartments in these cells (6, 23). To confirm this, we incubated polarized MDCK cells or PTCs expressing SNAP-Rab11a with apically added FITC-dextran for 20 min and then fixed and imaged the cells. As shown in Fig. 4, Rab11a in MDCK cells was present in a subapical cluster, as previously observed, and as expected, the majority of internalized dextran localized to small punctate compartments, consistent with early endosomes. In contrast, a much larger fraction of internalized dextran was present in Rab11a-positive compartments in PTCs [23.0 ± 3.9% in PTCs (n = 8) vs. 6.6 ± 1.6% in MDCK cells (n = 17), $P < 0.001$ by rank-sum test; Fig. 4] These results are consistent with the interpretation that apically internalized fluid-phase markers are largely segregated from membrane proteins in earlier compartments along the endocytic pathway in MDCK cells compared with PTCs.

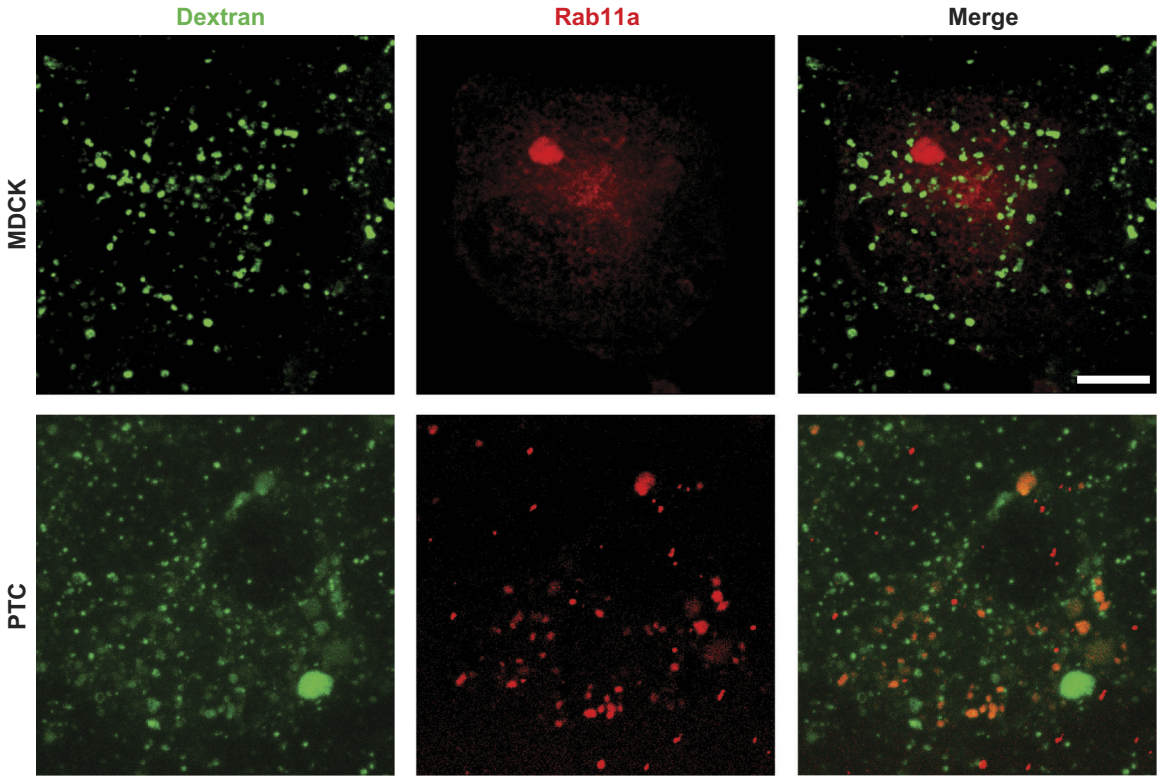

Fig. 4. Fluid-phase markers are not enriched in Rab11a-positive compartments in MDCK cells. Filter-grown MDCK cells (*top*) or PTCs (*bottom*) expressing *S*-nitroso-*N*-acetyl-penicillamine (SNAP)-Rab11a were labeled with tetramethylrhodamine (TMR)-Star and incubated with apically added FITC-dextran (1 mg/ml) for 20 min, fixed, and then examined by confocal microscopy. In contrast to the readily observed accumulation of dextran in Rab11a-positive compartments in PTCs, dextran has little access to this compartment in MDCK cells. Scale bar, 7.5 μm.

Ultrastructural analysis of AVs in rat kidney has revealed tubules emanating from these structures, suggesting that AVs may mediate sorting of membrane and fluid cargo (16, 17). To test whether Rab11a-positive structures in PTCs also undergo tubulation, we expressed SNAP-tagged Rab11a in PTCs by transient transfection, incubated cells with tetramethylrhodamine-SNAP to label Rab11a-positive compartments, and imaged living cells. As shown in Supplemental Movie S1 (see Supplemental Material for this article available online at the Journal website), Rab11a-positive structures were highly dynamic and were observed to undergo fusion and fission. Figure 5 and Supplemental Movies S1 and S2 show a tubule forming and dissociating from a Rab11a-positive structure. These data are consistent with the interpretation that Rab11a is a marker of the AV structures observed in vivo.

As noted above, albumin is thought to dissociate from megalin/cubilin in early endosomal compartments. We therefore asked whether albumin exits Rab11a-positive compartments in concert with a known fluid-phase marker (rhodamine-dextran). PTCs expressing SNAP-Rab11a were labeled with SNAP-Cell 505, incubated for 30 min with 40 μg/ml Alexa Fluor 647-albumin and 1 mg/ml rhodamine-dextran, and chased for 30 min. Cells were imaged in real time to visualize membrane dynamics. As shown in Supplemental Movies S3–S5, albumin and dextran were largely colocalized and readily detected in rapidly moving Rab11a-positive structures, as well as in tubular carriers containing both cargoes. While we speculate that these tubular carriers emanate from Rab11a-positive compartments, we were unable to unambiguously identify individual fission events.

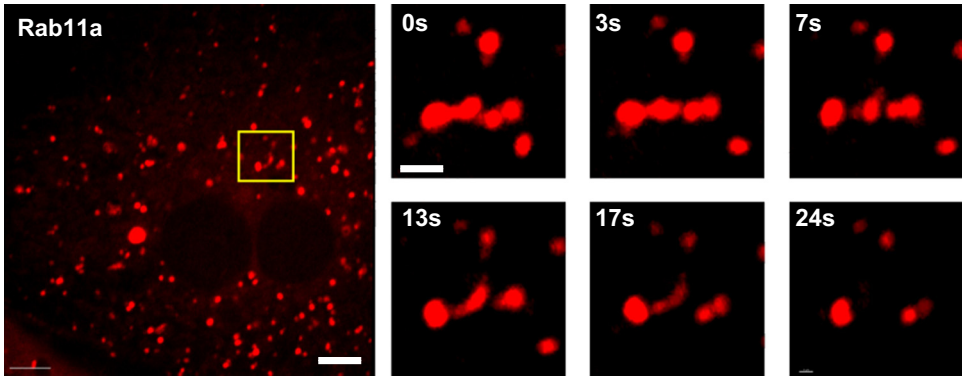

Fig. 5. Rab11a-positive compartments in PTCs are highly dynamic. PTCs cultured on MatTek dishes were transfected with cDNA encoding SNAP-tagged Rab11a. After 2 days, cells were incubated with Cell-SNAP TMR-Star to label the SNAP tag, washed, and then imaged by live-cell microscopy to visualize Rab11a dynamics. Rab11a localizes to multiple variously sized spherical compartments that are highly dynamic. *Left*: a representative cell. Scale bar, 7.5 μm. *Right*: time-lapse (0–24 s) images of a tubule emanating from the Rab11a-positive structure enclosed in the box in the image at *left*. Scale bar, 1 μm. (Movie from which these images are derived is available in Supplemental Material.)

Next, we assessed whether membrane and fluid-phase cargoes are sorted in Rab11a-positive compartments. We transfected PTCs with plasmids encoding Rab11a-SNAP and GFP-tagged truncated megalin (GFP-minimegalin), which retains the capacity to bind albumin (12, 32). Cells were incubated for 20 min at 37°C with Alexa Fluor 647-albumin and then imaged immediately (0 h) or after a 3-h chase (Fig. 6). GFP-minimegalin was detected at low levels on the cell surface and concentrated intracellularly in Rab11a-positive compartments. The distribution of this protein was qualitatively similar at 0 and 3 h, as expected for a protein at steady state (Fig. 6*A*). Quantitation of maximally projected confocal stacks confirmed this result: 67 ± 5.5% of the total GFP-minimegalin was present in Rab11a-positive compartments at 0 h vs. 63 ± 2.9% at 3 h (Fig. 6*B*). In contrast, more albumin was present in compartments containing Rab11a and GFP-minimegalin at 0 h than 3 h (Fig. 6*B*). Quantitation revealed a statistically significant drop in the total amount of albumin in Rab11a-positive compartments over this time period (from 35 ± 4.6% to 16 ± 1.6%, $P < 0.02$). Similarly, the amount of albumin colocalizing with GFP-minimegalin decreased from 33 ± 5.1% to 21 ± 2.6% ($P = 0.025$). Supplemental Movies S6–S8 illustrate the rapid dynamics of these cargoes in PTCs and confirm that heterologous expression of Rab11a in PTCs does not qualitatively alter the distribution or dynamics of GFP-minimegalin or albumin (see Supplemental Movie S9).

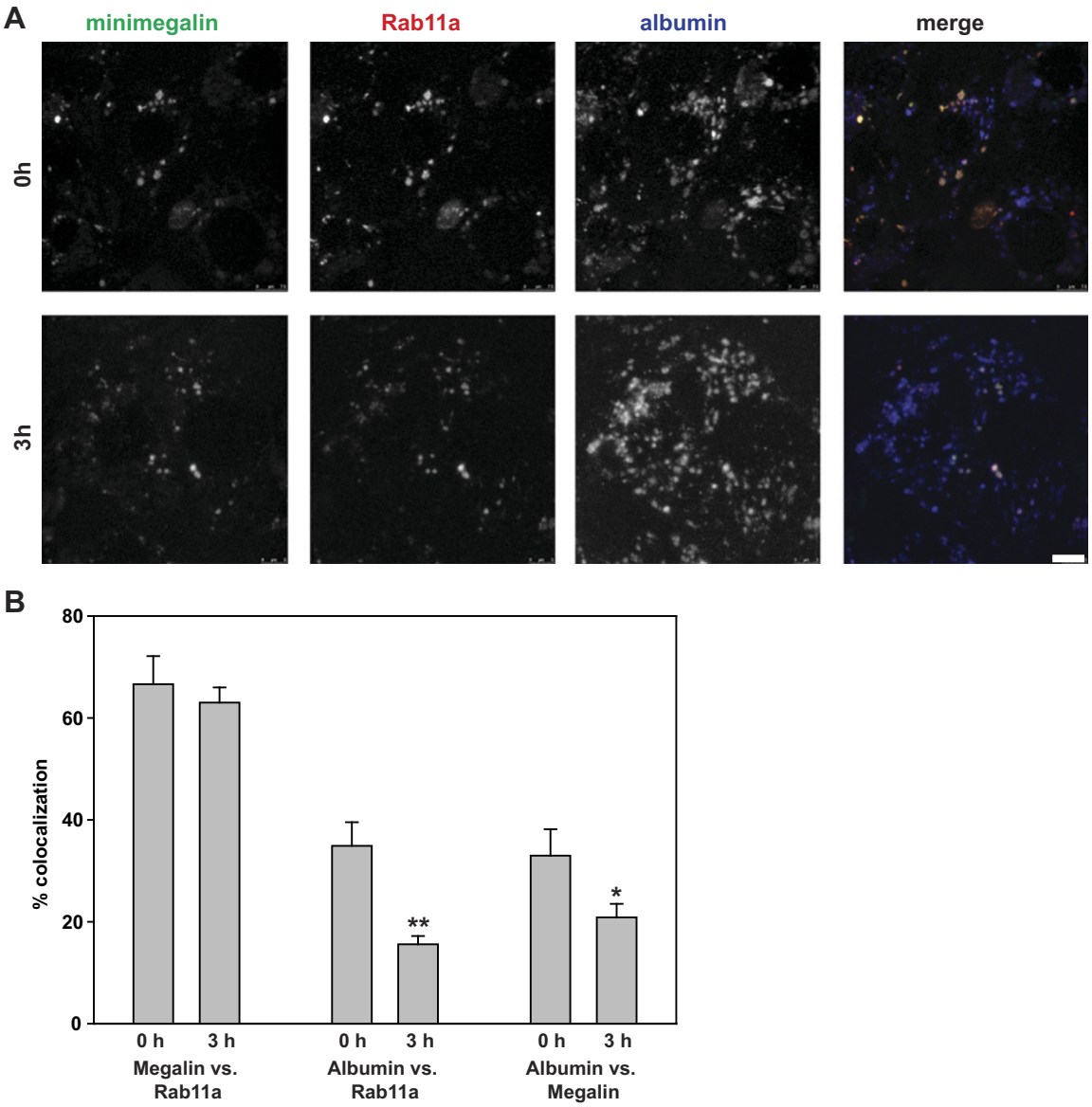

Fig. 6. Segregation of megalin and albumin in PTC Rab11a-positive compartments. *A*: PTCs grown on MatTek dishes were transfected with plasmids encoding mCherry-Rab11a and GFP-minimegalin. Cells were incubated with 40 μg/ml Alexa Fluor 647-albumin for 20 min, and confocal images of random fields were acquired immediately (0 h) or after a 3-h chase. Maximum projections of albumin, GFP-minimegalin, and Rab11a distribution, as well as merged images, are shown. Scale bar, 5 μm. *B*: amount of total cellular GFP-minimegalin in Rab11a-positive compartments and amount of albumin in Rab11a- or GFP-minimegalin-positive compartments in 6 images for each time point. Values are means ± SE. *$P = 0.014$; **$P = 0.025$ by Student's *t*-test. Whereas distribution of GFP-minimegalin does not change, albumin segregates from both markers during the chase period.

DISCUSSION

Despite the essential role of apical endocytosis in PT function, little is known about how the endocytic pathway is organized and regulated in PTCs. We have examined the organization of endocytic markers in primary cultures of PT. We found that Rab11a-positive compartments are dynamic structures that receive membrane and fluid-phase cargo internalized from the apical surface of PTCs. In contrast, apical endocytosis is far less robust in immortalized cells derived from other kidney segments. The unique morphology and function of Rab11a-positive compartments may reflect the high endocytic demands of PTCs compared with cells in more distal segments of the kidney tubule.

We used standard protocols to isolate primary cultures of PTCs. The resulting cell populations formed polarized monolayers with intact tight junctions and laterally localized E-cadherin. Moreover, ultrastructural analysis revealed the presence of subapical vacuolar structures consistent with those described previously in the PT. However, while our cells elaborated a few microvilli, they lacked the regular and highly differentiated brush border observed in vivo. Isolated PTCs expressed endogenous megalin, and subpopulations of cells could be distinguished on the basis of their expression of high levels of γ-GT (consistent with S2/S3-derived cells) or robust internalization of albumin (consistent with S1-derived cells).

We characterized the distribution of classical markers for endocytic compartments in PTCs. Whereas the morphology of early and late endosome/lysosome markers was not grossly different from that of other cell types, we found that the recycling endosome marker Rab11a localized to variously sized spherical compartments distributed throughout the cell. These structures are highly reminiscent of the AVs described in vivo and observed in our ultrastructural analysis. In contrast to this distribution, Rab11a is found primarily associated with the juxtanuclear recycling endosome and/or the *trans*-Golgi network in nonpolarized cells (35, 36) and with a subapical compartment termed the apical recycling endosome in polarized MDCK cells (8).

Rab11a-positive structures in PTCs were highly dynamic and were observed to undergo cycles of fusion and fission. Moreover, fluid-phase markers (rhodamine-dextran) and fluorescent albumin (which dissociates from megalin in acidic endosomal compartments) readily accessed these compartments. This is in contrast to observations in MDCK cells, where fluid markers are efficiently segregated from membrane proteins in early endosomes and are largely excluded from recycling endosomes (6, 23).

In vivo perfusion studies in rat kidney have determined that fluid-phase markers are internalized into tubular structures that may represent early endosomes and later appear in AVs (3, 9, 30). We attempted to determine whether internalized albumin and dextran appear in EEA1-positive early endosomes prior to reaching Rab11a-positive compartments, but our results were inconclusive. Thus it remains unclear whether there is a linear progression of cargo from early endosomes to Rab11a-positive compartments in our PTC cultures.

The differences we observed between cells from the PT and cells derived from other kidney segments have important consequences for our understanding of how this pathway is regulated in response to physiological need. In contrast to most other polarized epithelial cells [with the exception of intercalated cells of the kidney (22)], the PT is highly specialized for apical endocytosis. High apical endocytic capacity in the PT is required for the efficient internalization of filtered proteins, vitamins, and other solutes. Although the mechanism is unclear, we speculate that the unique size and geometry of Rab11a-positive compartments that we observed in PTCs enhance the segregation efficiency of internalized fluid and membrane cargoes to maintain robust PT apical endocytic capacity.

Importantly, many of the features essential for maintaining PT function are preserved in commonly used immortalized PTC lines. For example, apical endocytosis in OK and LLC-PK1 cells, derived from opossum and porcine kidney, respectively, is robust relative to basolateral internalization, similar to that observed in our primary cell culture model (unpublished data). Rab11a has been localized to the subapical region of OK cells (1), where recent higher-resolution images suggest that it is present in variously sized spherical compartments (7). Interestingly, these compartments become enlarged upon inhibition of class III phosphoinositide 3-kinase, and release of this block triggers rapid formation of tubular structures containing albumin (7).

The conclusions of our studies are limited by several technical shortcomings. *1*) Our cell cultures are relatively flat and lack a prominent brush border, suggesting that they have dedifferentiated to some extent. While our PTCs maintain a robust apical endocytic capacity, the regulation of this pathway likely does not exactly replicate that in vivo. For example, ultrastructural analysis of our cells did not reveal the prominent network of subapical tubules described in vivo (3, 17, 30). This network is also absent in immortalized PT-derived cell lines. *2*) While we confirmed by Western blotting that PTCs express endogenous Rab11a (not shown), we were unable, using multiple approaches, to confirm that the Rab11a-positive compartments we visualized correspond to the AVs described in vivo. *3*) Although we focused on "low-expressing" cells in our imaging studies (in high-expressing cells, Rab11a was distributed throughout the cytoplasm), it is possible that overexpression of Rab11a alters the normal sorting recycling pathway in our PTC cultures. Despite these caveats, our results provide important new information about the unique organization and function of the apical endocytic pathway in PTCs. Future studies are required to determine how the unique morphology of AVs facilitates efficient sorting and recycling to maintain PT function.

ACKNOWLEDGMENTS

We thank Dr. Carlton Bates and Caitlin Schaeffer for providing mouse kidneys and Dr. Ray Harris for advice and protocols for PTC isolation from kidney cortex. We are grateful to Dr. Donna Stolz, Jenny Karlsson, and Gregory Gibson (Center for Biological Imaging) and to the Kidney Imaging Core of the Pittsburgh Center for Kidney Research for assistance with ultrastructural analysis and live-cell imaging.

GRANTS

This work was supported by American Heart Association Grant 12SDG12040003 (to P. E. Mattila), National Institute of Diabetes and Digestive and Kidney Diseases (NIDDK) Grant R01 DK-54407 (to O. A. Weisz), and a NIDDK Pilot Grant from the Pittsburgh Center for Kidney Research (P30 DK-079307) to O. A. Weisz and P. E. Mattila.

DISCLOSURES

No conflicts of interest, financial or otherwise, are declared by the authors.

AUTHOR CONTRIBUTIONS

P.E.M., V.R., C.J.B., and O.A.W. are responsible for conception and design of the research; P.E.M., V.R., Y.R., and C.J.B. performed the experiments; P.E.M., V.R., Y.R., and C.J.B. analyzed the data; P.E.M., V.R., Y.R., and O.A.W. interpreted the results of the experiments; P.E.M., V.R., Y.R., and O.A.W. prepared the figures; P.E.M. and O.A.W. drafted the manuscript; P.E.M., V.R., Y.R., and O.A.W. edited and revised the manuscript; P.E.M., V.R., Y.R., C.J.B., and O.A.W. approved the final version of the manuscript.

REFERENCES

1. **Akhter S, Kovbasnjuk O, Li X, Cavet M, Noel J, Arpin M, Hubbard AL, Donowitz M.** Na^+/H^+ exchanger 3 is in large complexes in the center of the apical surface of proximal tubule-derived OK cells. *Am J Physiol Cell Physiol* 283: C927–C940, 2002.
2. **Bell CL, Tenenhouse HS, Scriver CR.** Initiation and characterization of primary mouse kidney epithelial cultures. *In Vitro Cell Dev Biol* 24: 683–695, 1988.
3. **Birn H, Christensen EI, Nielsen S.** Kinetics of endocytosis in renal proximal tubule studied with ruthenium red as membrane marker. *Am J Physiol Renal Fluid Electrolyte Physiol* 264: F239–F250, 1993.
4. **Bomsel M, Prydz K, Parton RG, Gruenberg J, Simons K.** Endocytosis in filter-grown Madin-Darby canine kidney cells. *J Cell Biol* 109: 3243–3258, 1989.
5. **Briere N, Martel M, Plante G, Petitclerc C.** Heterogeneous distribution of alkaline phosphatase and γ-glutamyl transpeptidase in the mouse nephron. *Acta Histochem* 74: 103–108, 1984.
6. **Brown PS, Wang E, Aroeti B, Chapin SJ, Mostov KE, Dunn KW.** Definition of distinct compartments in polarized Madin-Darby canine kidney (MDCK) cells for membrane-volume sorting, polarized sorting and apical recycling. *Traffic* 1: 124–140, 2000.
7. **Carpentier S, N'Kuli F, Grieco G, Van Der Smissen P, Janssens V, Emonard H, Bilanges B, Vanhaesebroeck B, Gaide Chevronnay HP, Pierreux CE, Tyteca D, Courtoy PJ.** Class III phosphoinositide 3-kinase/VPS34 and dynamin are critical for apical endocytic recycling. *Traffic* 14: 933–948, 2013.
8. **Casanova JE, Wang X, Kumar R, Bhartur SG, Navarre J, Woodrum JE, Altschuler Y, Ray GS, Goldenring JR.** Association of Rab25 and Rab11a with the apical recycling system of polarized Madin-Darby canine kidney cells. *Mol Biol Cell* 10: 47–61, 1999.
9. **Christensen EI, Birn H, Storm T, Weyer K, Nielsen R.** Endocytic receptors in the renal proximal tubule. *Physiology (Bethesda)* 27: 223–236, 2012.
10. **Christensen EI, Gburek J.** Protein reabsorption in renal proximal tubule-function and dysfunction in kidney pathophysiology. *Pediatr Nephrol* 19: 714–721, 2004.
11. **Cui S, Christensen EI.** Three-dimensional organization of the vacuolar apparatus involved in endocytosis and membrane recycling of rat kidney proximal tubule cells. An electron-microscopic study of serial sections. *Exp Nephrol* 1: 175–184, 1993.
12. **Cui S, Guerriero CJ, Szalinski CM, Kinlough CL, Hughey RP, Weisz OA.** OCRL1 function in renal epithelial membrane traffic. *Am J Physiol Renal Physiol* 298: F335–F345, 2010.
13. **Dunn KW, McGraw TE, Maxfield FR.** Iterative fractionation of recycling receptors from lysosomally destined ligands in an early sorting endosome. *J Cell Biol* 109: 3303–3314, 1989.
14. **Goligorsky MS, Hruska KA.** Transcytosis in cultured proximal tubular cells. *J Membr Biol* 93: 237–247, 1986.
15. **Gudehithlu KP, Pegoraro AA, Dunea G, Arruda JA, Singh AK.** Degradation of albumin by the renal proximal tubule cells and the subsequent fate of its fragments. *Kidney Int* 65: 2113–2122, 2004.
16. **Hatae T, Fujita M, Sagara H, Okuyama K.** Formation of apical tubules from large endocytic vacuoles in kidney proximal tubule cells during absorption of horseradish peroxidase. *Cell Tissue Res* 246: 271–278, 1986.
17. **Hatae T, Ichimura T, Ishida T, Sakurai T.** Apical tubular network in the rat kidney proximal tubule cells studied by thick-section and scanning electron microscopy. *Cell Tissue Res* 288: 317–325, 1997.
18. **Helbert MJ, Dauwe SE, Van der Biest I, Nouwen EJ, De Broe ME.** Immunodissection of the human proximal nephron: flow sorting of S1S2S3, S1S2 and S3 proximal tubular cells. *Kidney Int* 52: 414–428, 1997.
19. **Inoue CN, Sunagawa N, Morimoto T, Ohnuma S, Katsushima F, Nishio T, Kondo Y, Iinuma K.** Reconstruction of tubular structures in three-dimensional collagen gel culture using proximal tubular epithelial cells voided in human urine. *In Vitro Cell Dev Biol Anim* 39: 364–367, 2003.
20. **Jacobson HR, Kokko JP.** Intrinsic differences in various segments of the proximal convoluted tubule. *J Clin Invest* 57: 818–825, 1976.
21. **Kolb RJ, Woost PG, Hopfer U.** Membrane trafficking of angiotensin receptor type-1 and mechanochemical signal transduction in proximal tubule cells. *Hypertension* 44: 352–359, 2004.
22. **Lencer WI, Weyer P, Verkman AS, Ausiello DA, Brown D.** FITC-dextran as a probe for endosome function and localization in kidney. *Am J Physiol Cell Physiol* 258: C309–C317, 1990.
23. **Leung SM, Ruiz WG, Apodaca G.** Sorting of membrane and fluid at the apical pole of polarized Madin-Darby canine kidney cells. *Mol Biol Cell* 11: 2131–2150, 2000.
24. **Mattila PE, Youker RT, Mo D, Bruns JR, Cresawn KO, Hughey RP, Ihrke G, Weisz OA.** Multiple biosynthetic trafficking routes for apically secreted proteins in MDCK cells. *Traffic* 13: 433–442, 2012.
25. **McCaffrey MW, Bielli A, Cantalupo G, Mora S, Roberti V, Santillo M, Drummond F, Bucci C.** Rab4 affects both recycling and degradative endosomal trafficking. *FEBS Lett* 495: 21–30, 2001.
26. **Miedel MT, Weixel KM, Bruns JR, Traub LM, Weisz OA.** Posttranslational cleavage and adaptor protein complex-dependent trafficking of mucolipin-1. *J Biol Chem* 281: 12751–12759, 2006.
27. **Moestrup SK, Verroust PJ.** Megalin- and cubilin-mediated endocytosis of protein-bound vitamins, lipids, and hormones in polarized epithelia. *Annu Rev Nutr* 21: 407–428, 2001.
28. **Nielsen R, Christensen EI.** Proteinuria and events beyond the slit. *Pediatr Nephrol* 25: 813–822, 2010.
29. **Nielsen S.** Endocytosis in proximal tubule cells involves a two-phase membrane-recycling pathway. *Am J Physiol Cell Physiol* 264: C823–C835, 1993.

29a. **Okamoto CT.** *Don't wanna be Obama (all by my) self: Rab11a is involved in sequestration of fluid-phase cargo from membrane cargo*. Focus on "Rab11a-positive compartments in proximal tubule cells sort fluid-phase and membrane cargo." *Am J Physiol Cell Physiol* (January 15, 2014). doi:10.1152/ajpcell.00008.2014.

30. **Rodman JS, Seidman L, Farquhar MG.** The membrane composition of coated pits, microvilli, endosomes, and lysosomes is distinctive in the rat kidney proximal tubule cell. *J Cell Biol* 102: 77–87, 1986.
31. **Szalinski CM, Guerriero CJ, Ruiz WG, Docter BE, Rbaibi Y, Pastor-Soler NM, Apodaca G, Puthenveedu MA, Weisz OA.** PIP5KIβ selectively modulates apical endocytosis in polarized renal epithelial cells. *PLos One* 8: e53790, 2013.
32. **Takeda T, Yamazaki H, Farquhar MG.** Identification of an apical sorting determinant in the cytoplasmic tail of megalin. *Am J Physiol Cell Physiol* 284: C1105–C1113, 2003.
33. **Terryn S, Jouret F, Vandenabeele F, Smolders I, Moreels M, Devuyst O, Steels P, Van Kerkhove E.** A primary culture of mouse proximal tubular cells, established on collagen-coated membranes. *Am J Physiol Renal Physiol* 293: F476–F485, 2007.
34. **Trischler M, Stoorvogel W, Ullrich O.** Biochemical analysis of distinct Rab5- and Rab11-positive endosomes along the transferrin pathway. *J Cell Sci* 112: 4773–4783, 1999.
35. **Ullrich O, Reinsch S, Urbe S, Zerial M, Parton RG.** Rab11 regulates recycling through the pericentriolar recycling endosome. *J Cell Biol* 135: 913–924, 1996.
36. **Urbe S, Huber LA, Zerial M, Tooze SA, Parton RG.** Rab11, a small GTPase associated with both constitutive and regulated secretory pathways in PC12 cells. *FEBS Lett* 334: 175–182, 1993.
37. **Vergarajauregui S, Puertollano R.** Two di-leucine motifs regulate trafficking of mucolipin-1 to lysosomes. *Traffic* 7: 337–353, 2006.
38. **Verrey F, Singer D, Ramadan T, Vuille-dit-Bille RN, Mariotta L, Camargo SM.** Kidney amino acid transport. *Pflügers Arch* 458: 53–60, 2009.
39. **Weisz OA.** Acidification and protein traffic. *Int Rev Cytol* 226: 259–319, 2003.
40. **Wolff NA, Lee WK, Abouhamed M, Thevenod F.** Role of ARF6 in internalization of metal-binding proteins, metallothionein and transferrin, and cadmium-metallothionein toxicity in kidney proximal tubule cells. *Toxicol Appl Pharmacol* 230: 78–85, 2008.